Improved Supervisory Controller Design for a Fuel Cell Hybrid Electric Vehicle

Ali Molavi, Maria Serra Prat, Attila Peter Husar

***Abstract*—In this paper, a fuel cell system supervisory controller is developed for a fuel cell-based hybrid electric vehicle to safely control the interactions between powertrain components, maximize efficiency and minimize the degradation of the fuel cell. The proposed fuel cell supervisory controller includes three main elements: a state machine, an optimal setpoint generator and a power limit calculator. The state machine, as the top layer of the supervisory controller, is responsible for coordinating the various subsystems of the fuel cell, including the three subsystems, anode, cathode, thermal, and the DC/DC converter. The primary purpose of the state machine is to ensure global control over these subsystems as well as facilitate communication between the fuel cell system, diagnosis system, and Vehicle Control Unit (VCU). The state machine not only allows for the appropriate transitions between states but also governs the fuel cell system operation in all its different operating states such as Start-up, Shutdown and Run. The optimal setpoint generator is responsible for determining the operating conditions of the fuel cell system that maximizes the system's efficiency. It is designed by taking into account the comprehensive model of the fuel cell stack, considering manufacturing constraints, and incorporating the compressor map which then provides the optimal setpoints for all the subsystems' local controllers. A power limit calculator is also developed to compute the stack available power and feeds this information to the energy management system in the VCU. This information is used by the VCU to split the requested power between the fuel cell and the battery. The experimentally validated stack model and the complex model of the subsystems based on the Inn-Balance project data are used in the simulation. Furthermore, the subsystems' local controllers used in the MATLAB-Simulink were validated in a real vehicle test bench. The Common Artemis 130 km/h Driving Cycle (CADC) for automotive applications is used to verify the proposed fuel cell system supervisory controller in the MATLAB-Simulink environment. The simulation results showed that the proposed control structure functioned properly in the Run mode using this CADC-based load profile.**

***Index Terms*—Supervisory controller, PEM fuel cell, fuel cell hybrid vehicle, State machine, Optimal setpoint generator**

I. Introduction

FOSSIL fuels have played a major role in global economic growth, but their consumption causes harmful air pollution, as well as their limited supply, makes them unsustainable [1]. Transportation is a major contributor to this issue, accounting for approximately 24% of global greenhouse gas emissions in 2020, mainly from petroleum usage [2]. To address this, the transportation sector needs to become carbon neutral, and one potential solution is hydrogen as an energy vector. The decarbonization process can involve electrification, with hydrogen fuel cells playing a role [3]. Fuel Cell Hybrid Electric Vehicles (FCHEVs), which use fuel cells as the main energy generators and battery packs as secondary energy storage elements, have gained significant interest, particularly Polymer Electrolyte Membrane fuel cells (PEMFCs) due to their suitability for automotive and portable applications [4]. PEMFCs offer benefits like high energy density, safe operation, low noise, and fast startup [5]. However, PEMFCs face challenges related to cost, durability, and performance, which are crucial for commercialization and acceptance by end users [6]. Fuel cell degradation is primarily caused by extreme operating conditions, dynamic load profiles, improper operation during start, and stop cycles, idle modes, and contaminants in reactant gases. Idling, or high fuel cell voltages, accelerates catalyst corrosion, while start and stop processes can lead to reverse current and corrosion of the cathode catalyst carbon support, and in the presence of ice catastrophic damage in the stack can occur. Start and stop processes can cause the formation of a hydrogen-air interface in the anode that provokes reverse current and corrosion of the cathode catalyst carbon support [7]. Therefore, one of the most important areas of research in fuel cell systems is the integration of advanced control strategies and configurations to minimize these effects. These efforts aim to achieve a reliable dynamic response and maintain optimal operating conditions in alignment with the power requirements. The purposes of these strategies are to maximize efficiency and minimize the degradation of the fuel cell system.

The design of a fuel cell control system that is reliable, efficient and applicable in a real vehicle will be the focus of this paper. The main objectives of the fuel cell control system are: optimal reactants feedings, water management and heat management. During load changes, it is crucial to prevent reactant starvation as it is a major factor contributing to fuel cell degradation. Reactant starvation leads to severe corrosion of the carbon support, cell voltage reversal, and uneven current distribution, all of which can significantly impact the performance and lifespan of the fuel cell [8]. Water is necessary to humidify the membrane. However,

This work was supported in part by the Spanish State Research Agency through the Maria de Maeztu Seal of Excellence to IRI (MDM-2016-0656), and and in part by the Fuel Cells and Hydrogen 2 Joint Undertaking under Grant INN-BALANCE 735969. This Joint Undertaking receives support from the European Union's Horizon 2020 research and innovation program and Hydrogen Europe and N.ERGHY . Finally, the work acknowledges the support of the MAFALDA project funded by the Spanish Ministry of Science and Innovation (PID2021-126001OB-C31)

A. Molavi, M. Serra are with the Institut de Robòtica i Informàtica Industrial (CSIC-UPC), Llorens i Artigas 4-6, 08028 Barcelona. A.P.Husar is with the Department of Fluid Mechanics, Universitat Politècnica de Catalunya BarcelonaTech (UPC), Barcelona 08034, Spain. E-mail: ali.molavi, maria.serra, attila.husar@upc.edu

it is important to prevent situations where some parts are correctly hydrated, while others are too dry or overhydrated, as flooding can lead to blockage of reactants reaching the catalyst layer overhydrated, as this can lead to blockage of reactants [9]. Finally, it is important to maintain the operating stack temperature within the proper range. This is necessary to ensure optimal electrochemical reactions and preserve the integrity of the PEMFC stack material. Furthermore, non-uniform temperature distribution may cause condensation of water in the reactant gas channels [10].

In the past decades, considerable research has been dedicated to designing control strategies for fuel cell systems. The first part of the literature review primarily focuses on the current state of control strategies for individual subsystems in fuel cells, namely the thermal, anode and cathode subsystems. Subsequently, the review continues to examines works that focus on the design of controllers for the fully integrated fuel cell system.

Addressing thermal subsystem, the stack temperature control in [11] authors analyzed the temperature effect on an open-cathode self-humidified PEMFC. An extremum seeking algorithm was used to search for the temperature setpoint using the measured voltage, and a PI controller was used to manipulate the fan voltage. Fuzzy control is used in [12] to generate the cooling fan speed references. The temperature error, its derivative, and external load current are used as the fuzzy inputs. Lianghui Huang et al. in [13]] introduced dynamic inversion as a nonlinear strategy to regulate the temperature of a stack. This strategy involves manipulating the mass flow of coolant water to achieve the desired temperature control. Active Disturbance Rejection Control (ADRC) was used in [14] to compensate the uncertainty due to ambient temperature. Researchers adopted different water management strategies to maintain the electrolyte's degree of hydration at an optimal value and maximize the uniformity. A fault-tolerant control strategy is proposed in [15] to detect the state of health in terms of dryness and flooding. An adaptive neural network PID controller is proposed to regulate the inlet air stoichiometry to avoid the PEMFC from going into conditions of dryness or flooding. Differential flatness theory was used by Damour et al. [16]. In that work, using an experimental relation between membrane average water activity and cathode water activity, the desired value of the cathode mass of water is determined indirectly based on the expected value of the membrane water content, but there is no experimental validation. The impact of air stoichiometry and inlet air relative humidity was studied in [17],and a feedforward-feedback control configurations was proposed. Feedforward control was used to regulate the oxygen stoichiometry in response to load changes. Meanwhile, a feedback loop was employed to control the input voltage of the external humidifier, specifically with respect to the water content in the membrane.

Now focusing on the anode and cathode subsystem control strategies, the uneven distribution of gases on the electrode surface is a result of the slower speed of gas transmission compared to the rapid changes in current [8]. So, research communities proposed different control strategies to avoid gas starvation and uneven distribution. Tae-Hoon et al. in [18] proposed a dual closed-loop system with a static feedforward control structure to regulate the air supply fan. The feedforward control utilized a predefined map correlating the load current to the required air mass flow of the fan. This approach aimed to achieve equilibrium between water and heat within the stack, enhancing its performance and stability. In [19], a combined feedback and feedforward control strategy, along with an observer, was utilized to manipulate the input voltage of the compressor motor. The objective was to maintain constant air stoichiometry and achieve the desired net power in the fuel cell system. Due to the nonlinear nature of the system and uncertainties, nonlinear control strategies were proposed to achieve robustness to disturbances and parameter variations. Dalvi et al. in [20] used extremum seeking control strategy to maximize the efficiency of PEMFC and prevent oxygen starvation in an automotive application. Li et al. [21],introduced a sliding mode control strategy to regulate the air compressor's voltage to maximize the produced net power of a fuel cell system. Due to difficulties in obtaining an accurate model and the presence of un-modeled dynamics, model-free control strategies have been used by some studies. In [22], a comprehensive review of the application of machine learning and intelligent controllers for prediction, control, and energy management of hydrogen fuel cell vehicles was proposed. In [23], a robust adaptive controller based on Type-II Fuzzy Logic Systems (T2-FLS) was proposed to control the oxygen stoichiometry. Gheisarnejad et al. [24] introduced an adaptive Type-II fuzzy-based deep reinforcement learning control for oxygen stoichiometry in fuel cell systems. This algorithm exhibited better transient and steady-state response compared to sliding mode control, PI control, and fuzzy-based PI control. However, a substantial amount of data on the system's physical behavior was required for training the algorithm. Model Predictive Control (MPC), using a multivariable control strategy, has been widely applied by several authors to effectively control PEMFC systems while considering actuator limitations, state constraints, and output constraints. Sarmiento et al. [25] presented a decentralized model predictive controller for regulating reactant concentration in the anode and cathode channels of a fuel cell system. The approach was based on a distributed parameter model in the channel's direction. To address the challenge of quantifying degradation caused by reactant starvation, the authors suggested modeling the effective area where the reaction occurs. In [26],], a model predictive control approach is presented to maximize the Electrochemically Active Surface Area (ECSA).

When addressing the challenges of a fully integrated fuel cell system, one issue that arises is the potential operation of the fuel cell at unfavorable operating points. Therefore, it becomes crucial to identify the optimal operating conditions for different load power levels and ensure the fuel cell system operates within those conditions taking

into account all the subsystems. In the previous studies, the main objective was to control one or two parameters, such as the stack temperature [11]–[14], water management [15]–[17] and oxygen stoichiometry [18]–[21], [23], [24]. However, in real-world applications like automotive systems, achieving maximum efficiency requires the control of multiple parameters simultaneously. There are still challenges in obtaining and controlling the optimal operating conditions of a fuel cell stack specifically in automotive applications. The power requirements of a vehicle are constantly changing, resulting in varying current demands from the fuel cell system. To address this, it is essential to calculate optimal values for each requested power level. Additionally, real-time implementation of the algorithm necessitates a low computational burden to ensure efficient and timely operation. In the following, some studies addressing the operating condition optimization and evaluation are reported. Maximizing the net power and the exergetic efficiency was studied in [27]. They used a semi-empirical fuel cell stack model and an associated balance of plant model to obtain the optimal operating conditions. They did not consider the water management and humidity ratio of the inlet air and hydrogen in their optimization problem. Wu et al. [28] presented an optimization approach to determine the optimal values of four variables: cell temperature, cathode stoichiometry, cathode pressure, and cathode relative humidity. The goal was to maximize the overall efficiency of the fuel cell system across various current densities. However, the proposed method was not tested in a real system to evaluate computation time. In the study by Nanadegani et al. [5], a neural network model for the fuel cell stack is proposed. This model is used to calculate the optimal values of operating parameters such as relative humidity, anode and cathode stoichiometry, and temperature. Their objective was to find the optimal parameter values for different current densities to maximize and minimize the output power. The pressure was assumed to be constant for anode and cathode. However, the cathode pressure influences the output power and should be considered. In [29], a model predictive control based on an observer to maximize efficiency and minimize the degradation of a PEMFC systems was presented. The control strategy proposed by the researchers aims to prevent fuel and air starvation, maintain appropriate humidification levels, maximize overall efficiency, and optimize the electrochemical active surface area. This is achieved by controlling variables such as current, coolant water mass flow, air relative humidity, and hydrogen mass flow.

To obtain a response that closely mimics the behavior of a real system, it is necessary to consider a detailed model that encompasses all the balance of plant subsystems, including components such as valves, fans, compressors, radiators, pipes, and hydrogen ejector-injectors. This comprehensive modeling approach ensures a more accurate representation of the system dynamics and enhances the fidelity of the response. However, this kind of models are not found in the literature. Moreover, to the best of the author's knowledge, there is a scarcity of studies in the existing literature where researchers have proposed a supervisory controller that not only determines optimal operating conditions for the fuel cell stack and setpoints for subsystems but also provides a systematic approach for managing the overall fuel cell system functionality, including startup and shutdown procedures. Furthermore, limited research has been conducted on the application of state machine-based control for fuel cell systems, specifically in the automotive field. Previous applications of state machines have primarily focused on energy management systems [30], [31]. Additionally, this work will present the importance of minimizing stack degradation by estimating the available power of the stack and feeding this information to the vehicle's energy management system (EMS). The EMS then utilizes this data to restrict the power requested from the fuel cell system within the estimated available power range.

The main objective of this paper is to develop a fuel cell supervisory controller using a detailed and experimentally validated fuel cell system model. The designed controller will be implemented in MATLAB/Simulink, and its performance will be evaluated through simulation experiments. The supervisory controller consists of three main components. Firstly, a state machine facilitates global coordination and communication among the subsystems. Secondly, an offline optimal setpoint generator computes operating conditions that maximizes efficiency while considering all manufacturer limitations to minimize degradation. Lastly, a power limit calculator estimates the immediate and future power capabilities of the fuel cell stack based on measured stack variables and determines the DC/DC converter current setpoint. The main contributions of this paper are summarized as follows:

- In this study, an improved model, based on the INN-BALANCE project's fuel cell system is employed [32]. This model incorporates all the sensors and actuators present in the real system and has been experimentally validated. Notably, the model introduces an equivalent electric circuit model with distributed parameters for the cell. This allows for the accurate representation of the stack's voltage during galvanostatic mode, which is the operating mode of the automotive application in the normal run state.
- Propose a state machine architecture as a basic structure that contains all the operating states required to manage the PEMFC system processes in the vehicle, such as the Startup, Shutdown, and Run.
- Design a power limit calculator to estimate the available stack power for the vehicle control unit's energy management.
- Determine the setpoint current for the DC/DC converter based on the measured airflow entering the cathode channel. In this manner, the controller ensures a safe electric current applied to the stack while considering the dynamic behavior of the compressor and prevents oxygen starvation.
- Design an off-line setpoint calculator based on a detailed model of the fuel cell stack.

- Evaluate the proposed supervisory controller using the Common Artemis 130kph Driving Cycle (CADC) and the detailed model of all the major balance of plant components from the INN-BALANCE project.

The paper is organized into the following sections. Section II is assigned to the description of the fuel cell system model. In section III, the fuel cell system supervisory controller is described, which includes optimal setpoint generator, state machine, and power limit calculator. Section IV is dedicated to the simulation results and verification of the proposed supervisory controller integrated with the experimentally validated stack model and balance of plant subsystems model. Finally, in section V the main conclusions and key results are summarized.

II. Fuel Cell System Dynamic Model

A. General scheme of the PEMFC system

A mathematical model of the system is needed to design the fuel cell system supervisory controller. Fig. 1 shows the fuel cell system studied in this work, that includes five auxiliary subsystems, i.e., anode, cathode, thermal, electronic subsystems and the PEMFC stack. The hydrogen is stored in a pressurized tank and is delivered to the stack anode channel through the anode subsystem. The anode subsystem also includes a hydrogen recirculation loop to increase the utilization rate of hydrogen [1]. The cathode subsystem is responsible for delivering the demanded air flow to run the fuel cell. It is equipped with an air compressor that supplies air at the desired pressure and a humidifier to properly humidify the inlet air [33]. The operating stack temperature has to be kept in the proper range to maintain optimum electrochemical reactions and keep the integrity of the PEMFC stack material. The thermal subsystem recirculates coolant to remove the generated heat [34]. Finally, the power electronic subsystem is in charge of the electric power conditioning.

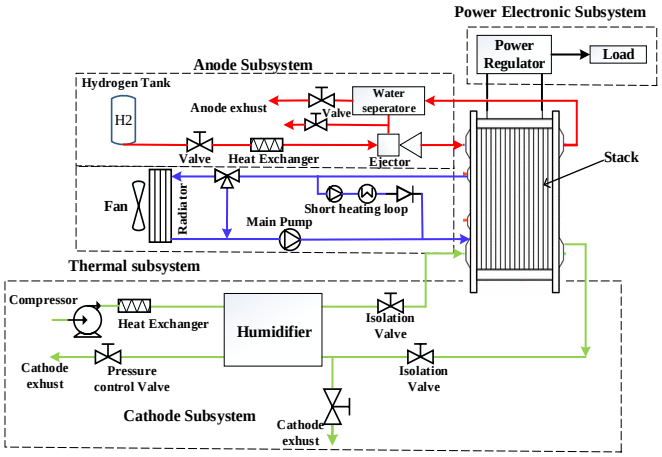

Fig. 1. Balance of Plant schematics of fuel cell system and the auxiliary subsystems

B. PEMFC stack model

The PEMFC stack is an assembly of $N_C = 335$ single cells. Each cell in the stack is modeled using a $1+1D$ parameter model. The gas flow transports along the channel are described with discretized Δz, and the transports in the direction perpendicular to the membrane are considered lumped parameters, except for the Gas Diffusion Layer (GDL) where different volumes are considered. Therefore, the GDL is discretized in two directions. This consideration allows to implement model-based control strategies that take into account the internal species concentration profiles in fuel cell, which is important to avoid starvation and improper reactants distribution, and water distribution. The main fuel cell parameters are shown in Table I. More details can be found in [35].

TABLE I
Stack Parameters

Parameter	value	Parameters	value
Channel length	0.4 m	Fuel cell stack gross power	100kw
Channel width	1 mm	PEM fuel cells active area	300cm2
Channel depth	0.7 mm	Maximum operation current	450Amp
Z-Direction discretization points	3	Number of cell (N_c)	335
Y-Direction discretization points GDL	3	T_{ref}	340 K
C^A	$8.25 \times 10^6 Fm^{-3}$	C^C	$8.25 \times 10^6 Fm^{-3}$
δ^{AC}	$4 \times 10^{-5} m$	δ^{CC}	$1.1 \times 10^{-4} m$

1) Electrochemical Model: The automotive PEMFC system described in this paper works in galvanostatic mode during normal operation when power is produced, known as the Run state. The DC/DC converter sets the current that circulates through the stack which is based on the power limit calculator. In order to have the same causality in the stack model, the current is a model input and the voltage is calculated as the model output. The stack operating voltage V_{fc} is calculated as the total sum of the N_c single-cell voltages as follows.

$$V_{fc} = N_c U \tag{1}$$

where N_c is the number of cells. The cell voltage U is composed of the voltage drop in the cathode, anode and membrane as follows [35].

$$U = \Delta\Phi^C - \Delta\Phi^A - \Delta\Phi^M \tag{2}$$

where the voltage drop at the cathode side and anode side, $\Delta\Phi^C$ and $\Delta\Phi^A$, are computed based on (3) and (4). They depend on the reaction rates at catalyst layers(CL), $r^A(z)$ and $r^C(z)$, and their physical characteristics [36].

$$\Delta\dot{\Phi}^A(z) = \frac{i^{st}(z) - 2Fr^A(z)}{C^A \delta^{AC}} \tag{3}$$

$$\Delta\dot{\Phi}^C(z) = \frac{2Fr^C(z) - i^{st}(z)}{C^C \delta^{CC}} \tag{4}$$

being C^A and C^C are the volumetric capacitance of the anode and cathode CL, respectively. i^{st} is the mean current density through the stack. The y-direction thickness of the anode and cathode catalyst layer (CCL) is represented by δ^{AC} and δ^{CC}. The voltage drop in the membrane, $\Delta\Phi^M$, depends on the membrane water content, Λ, gradients of water concentration and protons H_+, and the current density i^{st} as Eq.(5).

$$\Delta\Phi^M = \frac{\delta^M}{\sigma(\Lambda)} i^{st} + \frac{\delta^M}{F} t_w(\Lambda) \Delta\mu_{H_2O} + \frac{\delta^M}{F} \frac{RT_{cell}}{\xi_{H_+}(\Lambda)} \Delta\xi_{H_+} \tag{5}$$

where $\Delta\mu_{H_2O}$ is the water chemical potential gradient, $\Delta\xi_{H_+}$ the proton mole fraction gradient, and ξ_{H_+} is the proton mole fraction. More details about these parameters can be found

in [36]. The mean current density through the stack, $i^{st} = I_{st}/A_{cell}$, is known, where I_{st} is the stack current. However, the voltage U and the distribution of current density i_j^{st} in the membrane are unknown. To obtain the current density i_j^{st} at any discretization point j, an equivalent electric circuit for the cell is considered, as shown in Fig. 2 The electrical branches

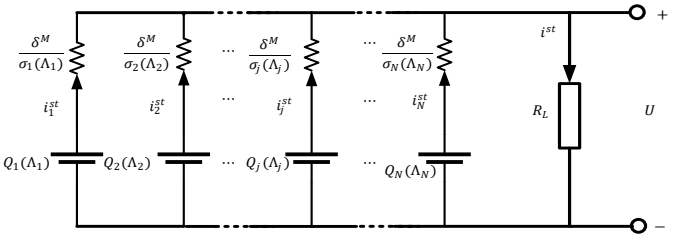

Fig. 2. Cell equivalent circuit

represent the different discretization points. R_L represents the external load resistance. The j subscript denotes the jth discretization point, and N is the number of discretization points. Each branch has an equivalent source voltage, Q_j, shown in (6), and a variable resistance that depends on each discretization's water content. The aforementioned equivalent electric circuit can be expressed in matrix notation as seen in (7).

$$Q_j = -\frac{\delta_j^M}{F} t_w\left(\Lambda_j\right)\left(\Delta\mu_{H_2O}\right)_j - \frac{\delta_j^M}{F}\frac{RT_{cell}}{\xi_{H_+}\left(\Lambda_j\right)}\left(\Delta\xi_{H_+}\right)_j + \Delta\Phi_j^C - \Delta\Phi_j^A \tag{6}$$

$$\mathbf{A}\mathbf{i}^M = \mathbf{B} \tag{7}$$

where matrixes A and B are calculated as follows:

$$\mathbf{A} = \begin{bmatrix} \frac{\delta^M}{\sigma(\Lambda_1)} & -\frac{\delta^M}{\sigma(\Lambda_2)} & 0 & \dots & 0 \\ \frac{\delta^M}{\sigma(\Lambda_1)} & 0 & -\frac{\delta^M}{\sigma(\Lambda_3)} & \ddots & 0 \\ \frac{\delta^M}{\sigma(\Lambda_1)} & \vdots & \vdots & \ddots & \vdots \\ \frac{\delta^M}{\sigma(\Lambda_1)} & 0 & 0 & 0 & -\frac{\delta^M}{\sigma(\Lambda_N)} \\ 1 & 1 & 1 & 1 & 1 \end{bmatrix} \tag{8}$$

$$\mathbf{i}^M = \begin{bmatrix} i_1^{st} \\ i_2^{st} \\ i_3^{st} \\ \vdots \\ i_N^{st} \end{bmatrix}, \ \mathbf{B} = \begin{bmatrix} Q_1 - Q_2 \\ Q_1 - Q_3 \\ \vdots \\ Q_1 - Q_N \\ N i^{st} \end{bmatrix}$$

The coefficients of matrix $\mathbf{A}$, represent the electrical resistivity of each discretization point along the membrane. As long as the conductivity's in matrix $\mathbf{A}$ are strictly positive, $\sigma(\Lambda_j) > 0$, the liner matrix equation $\mathbf{i}^M = \mathbf{A}^{-1}\mathbf{B}$ is solvable. Q_j are auxiliary variables used to represent the voltage on the discretization point and they are defined as follows:

$$Q_j = U + \frac{\delta^M}{\sigma(\Lambda_j)} i_j^{st} \tag{9}$$

So, by having the distribution of current in the membrane, i_j^{st}, and using Eq. (6), the cell voltage U is obtained. The exchange current density at the cathode, i_0, is a function of the fuel cell temperature T_{cell}, oxygen parpressure at the CCL, and the electrochemically active surface area at the CCL (ECSA) [35], [37]. It is calculated as follows:

$$i_0 = i_{0,ref}\frac{ECSA}{A_{geo}}\left(\frac{p_{O_2}}{p_{O_2,ref}}\right)^{0.5} e^{\left[-\frac{\Delta G^*}{RT_{cell}}\left(1-\frac{T_{cell}}{T_{ref}}\right)\right]} \tag{10}$$

where $i_{0,ref}$ is the intrinsic catalytic Pt activity at conditions T_{ref} and $p_{O_2,ref}$. A_{geo} is the total surface area of the electrode, and ΔG^* is the Gibbs activation energy for the oxygen reduction reaction at the CCL. These parameters are obtained from the experimental validation with the provided data by INN-BALANCE partner PowerCell[1]. The dynamic equations that describe the mass balance of gas species at the gas channels and the gas diffusion layers, as well as the anodic reaction rate and the cathodic reaction rate were developed in [36], [38]. In the following section, the liquid water in the cathode catalyst layer is modeled and the effect of this liquid water in ECSA and finally in the output voltage is described.

2) Liquid water in Cathode Catalyst Layer (CCL): In [26], the liquid water in the CCL is modeled with the mesoscopic pore filling effects of the CCL structure. Given that the data acquired from the fuel cell stack does not include this information. A simpler version of the S is proposed in this work. Here, S, is defined as the volume of liquid water over void volume in the CCL. The S dynamics depends on the rate at which the liquid water is evaporated, I_{evap}, and the generation of liquid water on the CCL, $\dot{n}_{H_2O}^C$ which is the flux of the cathodic reaction rate. S dynamic is defined as follows:

$$k_s\frac{dS}{dt}(z) = I_{gen}(z) - I_{evap}(z) = \dot{n}_{H_2O}^C(z) - I_{evap}(z) \tag{11}$$

$$I_{evap}(z) = K_{evap}\frac{S(z)\left(p^{sat}(z) - p^{vap}\right)}{RTA_{pore}}, \ if \ p^{vap}(z) < p^{sat} \tag{12}$$

where K_{evap} is the evaporation time constant, p^{sat} is the saturation pressure, p^{vap} is the vapor partial pressure at the GDL, A_{pore} is the pore surface area per unit volume of the GDL/CL, and k_s is the liquid water accumulation time constant. The electrochemically active surface area is defined as follows:

$$ECSA(z) = A_{ref}e^{(k_{act}S-1)} \tag{13}$$

where A_{ref} is the reference area multiplier and k_{act} is the active area reduction coefficient.

C. Subsystems model

As Fig. 1 shows, the fuel cell stack can not stand alone and needs different BoP elements, grouped into three main subsystems; cathode, anode and thermal subsystems.

1) Cathode subsystem: The cathode subsystem was developed by BROSE[2], which is in charge of delivering the demanded air flow with the desired pressure, stoichiometry, and humidity ratio.

[1]PowerCell, Sweden AB
[2]Brose Mechatronics, Germany

2) Anode subsystem: The anode subsystem was designed at AVL[3], and it provides the flux of hydrogen from the H_2 tank to the fuel cell. The anode subsystem controls the pressure at the inlet of anode channel to continuously track the cathode channel inlet pressure plus 0.2 bar, as indicated by the fuel cell manufacturer.

3) Thermal subsystem: The PEMFC in this project is designed to operate with a maximum temperature difference between the inlet and outlet under normal operating conditions from 68º to 80º Celsius. The thermal subsystem, which is responsible for the stack temperature control, was developed by DLR[4].

III. Supervisory Controller Design

In this section, a novel fuel cell system supervisory controller is proposed and described. Supervisory controllers distribute the system's global demands to specific demands required from individual subsystems or components. Usually, the individual demands are translated into the setpoints for the local controllers, which are well-tuned for closed-loop stability [39]. Additionally, complex systems like vehicles have different states of operation, each corresponding to different functions. Hence, in a vehicle, there are many different states as the Startup, Run, Shutdown and, Idle. The proposed fuel cell supervisory controller integrated with the different elements of the car propulsion system is shown in Fig. 3. As it can be seen, the fuel cell hybrid electric vehicle overall system architecture is divided into different layers. The highest level of control is the Vehicle Control Unit (VCU), which works as the central controller. The second level, which is the focus of this work, is the fuel cell system supervisory controller. It comprises three main parts; State Machine (SM), Optimal Setpoint Generator (OPSG) and Power Limit Calculator (PLC). The fuel cell system supervisory controller developed in this work is a hybrid control architecture. It includes a discrete event control system that decides when to activate different operating states and substates. Additionally, it incorporates a optimal setpoint generator which is responsible for continuously generating appropriate setpoints for the local controllers of the subsystems. The discrete event controller of this work is a state machine developed with Stateflow and the continuous control system is implemented as an optimal setpoint generator linked to the local controllers. Furthermore, the supervisory controller also includes an algorithm to estimate the available stack power which is the Power Limit Calculator. The supervisory controller receives all the information from the input wrapper, which collects 33 input signals. These includes orders from the VCU, estimation from the observer, and diagnostic results from the diagnostic unit. The supervisory controller uses the collected information to automatically coordinate the subsystems, determines local controller setpoints, determines DC/DC converter current setpoint, and estimates the stack available power information for VCU. The diagnosis unit is in charge of diagnosing the hardware failure, such as sensors failure, compressor errors, etc. If a failure is detected, the diagnosis unit will inform the state machine, and the state machine puts the fuel cell system in the normal Shutdown, fast Shutdown, or the Failsafe following a safe procedure. The third level includes the ancillary subsystems' local controllers, i.e., anode, cathode, and thermal subsystems' controllers. Each subsystem controller (SSC) is programmed with local control algorithms to achieve the setpoints received from the fuel cell system supervisory controller at the upper level. The lowest level comprises the fuel cell stack, DC/DC converter, cathode subsystem, anode subsystem and thermal subsystem.

[3]AVL List GmbH, Engineering Service Provider
[4]DLR Stuttgart, German Aerospace Center

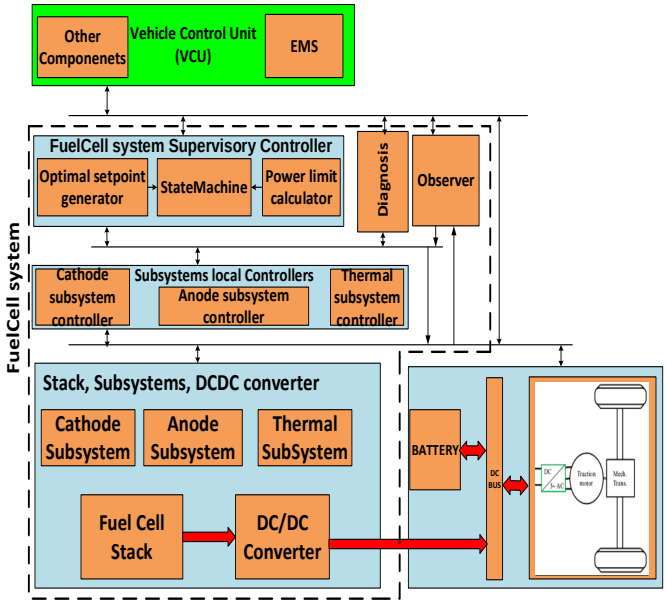

Fig. 3. Relation of the proposed supervisory controller along side other components in the fuel cell hybrid electric vehicle's overall system architecture

A. State machine architecture

The central part of the fuel cell supervisory controller is the state machine. The state machine combines time and event-triggered actions and allows issuing messages in an event-based style [40]. It is based on "if-then-else" logic and has the typical state machine advantages. First, explicitly readable and relatively easy to identify the condition of the supervisory controller. Second, simple to calibrate because of the limited number of parameters [41]. The state machine in this work is adopted as the basic control structure and contains all the operating states and substates of the PEMFC system processes. It ensures the orderly flow of events and prevents the occurrence of undesired chains of events in the system. The state machine also contains the conditions required to transit from one state to another. All transitions are triggered based on exogenous and internal signals such as timers, to ensure safe operation and effective use of the resources. If the state machine is in a particular state, such as "Run," that state manages the inputs and outputs. It is capable of reading from all inputs of the state machine and writing to all outputs. The cathode, anode, thermal, and DC/DC converter subsystems have multiple modes. During various states of operation of the fuel cell system, such as Startup, Shutdown,

and Run, those subsystems should operate in specific modes. So, they need to be informed about their operation modes. To deal with this requirement and establish a communication channel between the fuel cell supervisory controller and the subsystems local controllers, the protocol numbers and the status numbers are defined. The protocol numbers are used by the supervisory controller to order the different subsystem and the status numbers are used by the subsystems to report their operation modes and status. In summary, the inputs of the state machine include the optimal setpoints from the optimal setpoint generator, VCU control signals such as position of the key and the state of operation, the status number of the different subsystems, diagnosis signals, and some measurement signals such as the stack current, stack temperature and the ambient temperature. The outputs of the state machine include the protocol numbers to all subsystems, the setpoints of the subsystems, and error detection flags that are implemented within the state machine. Depending on the state of operation and based on the implemented algorithm inside of the state machine, which is not focus of this paper, specific values are assigned to each output.

1) State machine states: The proposed state machine consists of the following states: Initialization, Failsafe, Standby, Refueling, Service Mode, Startup, Run, Minimum power, Normal Shutdown and Fast Shutdown. The state-chart diagram of the proposed state machine is shown in Fig. 4. In the

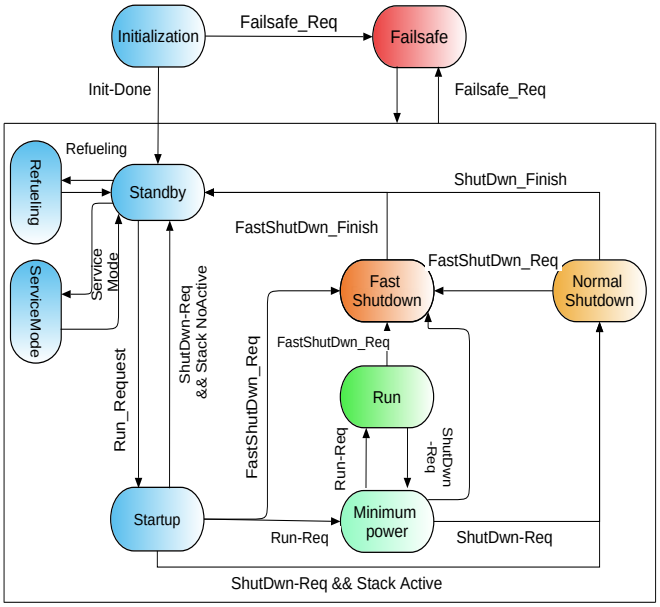

Fig. 4. State-chart diagram of the proposed state machine for the fuel cell system

following paragraphs, the behavior of the state machine is presented with a walk through the state machine from the Startup to the Shutdown. The fuel cell supervisory control unit is turned on when the vehicle is opened and the on-board computer turns on. The state machine starts in the initial state called Initialization, during which all the subsystems are turned off. If the different subsystems' initialization is done correctly, the state machine moves to the state Standby and waits until the Run-Requested is activated by the VCU. If Run-requested is activated, the state machine transitions to the next states where the Startup procedure begins. During the Startup procedure, the state machine sends the protocol numbers and setpoints to the subsystem controllers in order to start the different subsystems. The state machine receives feedback from the subsystems through the sensors and the status variables. At the end of the Startup procedure, both the subsystems and the fuel cell are ready to operate in Run mode. During Run state, the task to control the subsystems is delegated to the setpoint generator. The setpoint generator updates the subsystems' setpoints based on the requested power, while the power limit calculator updates the DC/DC converter current reference based on the the amount of air available in the stack. During the Run state, the state machine receives these setpoints and assign them for the respective subsystems and the DC/DC converter. When necessary, the driver stops the car and the system transitions to the Minimum power state. From this state, the system can either go to the Startup procedure again or proceed to the Shutdown. In the Shutdown process, the subsystems have to be turned off in an orchestrated manner by receiving ordered protocol numbers to avoid damages in the fuel cell stack, and the state machine returns to the Standby state. In the case of malfunctioning in one subsystem or an equipment, the Failsafe mode is triggered and all the equipment are depowered. The Failsafe mode has the highest priority among the other states of operation.

B. Optimal setpoint generator

In order to make PEMFC competitive, one of the most important research efforts is the integration of control strategies that ensure optimal operating conditions, maximizing efficiency, and preventing degradation based on the required power. In the previous work [42], an offline optimal setpoint generator was proposed. It is executed during the Run state and generates the setpoints for auxiliary subsystems based on the requested power from the vehicle side. These setpoints are designed to maximize the efficiency of the PEMFC. The controlled variables includes cathode mass flow, cathode humidity ratio, cathode inlet pressure and outlet coolant temperature. In this paper, the previous offline optimal setpoint generator in [42] has been updated to incorporate a new range of cathode inlet air humidity ratio. Additionally, It takes into account the power consumption of the fans, pumps and compressor in the auxiliary subsystem. The humidifier considered in the INN-Balance project has the range of humidity ratio smaller than the range reported in [42]. The PEMFC efficiency is computed as follows:

$$\eta = \frac{P_{net}}{HHV \cdot \dot{n}_{H_2}} = \frac{IV_{fc} - \sum_{s=subsystems} P_s}{HHV \cdot \dot{n}_{H_2}} \tag{14}$$

where $\dot{n}_{H_2}$ is the fuel out of the H_2 tank, and *HHV* is the higher heating value of the fuel. IV_{fc} is the gross electrical power generated by the fuel cell and P_s is the electrical power consumed by the subsystems.The consumption of the subsystems includes the power consumption of the compressor and a constant power consumption for the other auxiliary subsystems. Therefore, the efficiency depends on hydrogen flow out of the tank, fuel cell gross power, and the subsystems

consumption. The second control objective is to minimize degradation. This objective is achieved by complying with the manufacturers' constraints on the PEMFC stack and subsystems.

1) Optimal subsystems setpoints: The optimization problem to be solved is described in (15):

$$\begin{aligned} &maximize \quad \eta(r)\,|I_{st} \\ &r_1, r_2, ..., r_6 \\ &subject\ to \quad \frac{r_i \leq r_i \leq \overline{r_i}}{W \cdot r \leq Y} \end{aligned} \tag{15}$$

where η is the efficiency, $\overline{r_i}$ and $\underline{r_i}$ are the lower and higher boundaries, and (W, Y) are the inequality constraints due to compressor map. The experimentally validated stack model is run until steady state is achieved for all possible combinations of valid setpoints within a finite grid. This process allows for the creation of a comprehensive map of the operating region. The compressor map, which relates the pressure ratio to the mass flow rate, limits the setpoint's possible value in the compressor's operation space. The efficiencies are evaluated for each group of setpoints, and the setpoint values that maximize the efficiency are chosen as the optimal setpoints at each stack current. The result of the evaluation can be found in Table II. The anode inlet overpressure relative to cathode inlet pressure and inlet coolant temperature have constant values. The cell voltage, the output net power, and the efficiency for the maximum efficiency points are shown in Fig. 5. All the data samples form vertical lines, and the maximum efficiency points at each current are connected with a blue line. The effect of considering the power consumption of auxiliary equipment such as fans and pumps is shown in the efficiency plot. The green curve shows the effects of considering this consumption comparing it with blue curve, which ignores it. As Table II

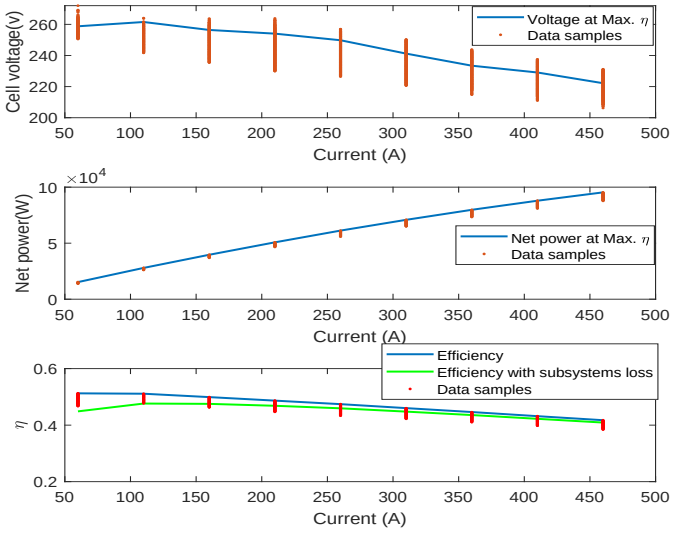

Fig. 5. Cell Voltage, Net produced power and Efficiency

shows, the mass flow rate and cathode inlet pressure increase with an increase in the demanded load current. Additionally, the generated water increases due to the increase in the reaction rate. So, to prevent the flooding phenomenon, an increase in the temperature setpoint and decrease in the external humidification setpoint is observed.

C. Power Limit Calculator

One of the duties of the fuel cell system supervisory controller (FCSSC) is to compute the available range of power that the fuel cell stack can deliver and send this information to the energy management system of the vehicle control unit. The energy management system uses this information to manage the power requested by the traction components, distributing this power between the fuel cell stack system and the battery. The information delivered by the fuel cell system supervisory controller to the energy management system includes maximum power, DC/DC setpoint current, maximum power ramp-up rate, and maximum instant power.

1) Maximum power: The maximum power is the maximum net power that the fuel cell is anticipated to deliver, assuming sufficient time to adjust the fluid dynamic state, considering the current stack temperature and membrane hydration conditions. The maximum power is the value that will limit the power supplied by the fuel cell system. Due to the slower dynamics of the stack temperature and hydration conditions in comparison to the dynamics of the air compressor, the time constants of the stack temperature and hydration condition are larger than those of the inlet air pressure and mass flow rate, which are less than 3 seconds. The stack temperature and hydration conditions, represented by the ECSA, are the only parameters that influence the maximum power. The ECSA is a measure of the total active Pt available in the carbon-support layer at the cathode CL (CCL), and it depends on the Pt loading of the CCL, the pore distribution, the CCL hydration state, and the degradation condition of the stack [26]. Hence, the ECSA serves as an effective indicator to reflect the hydration state of the stack. The stack temperature, which is considered to be equivalent to the temperature of the coolant at the outlet, is measured. However, the ECSA cannot be measured and needs to be estimated. The use of ECSA observer based on the distributed model of the stack would increase the computational burden for the real time implementation [26]. Therefore, a new simpler algebraic solution is proposed in this work. Considering the Butler-Volmer voltage equation (16), (17) and the exchange current density i_0 in (10)

$$V_{cell} = E_r - \frac{RT}{\alpha 2F}\left[log\left(\frac{i}{i_0}\right) - log\left(\frac{p_{O_2}}{p_{O_{2,ref}}}\right)\right] - R_{ohm}i \tag{16}$$

$$E_r = E^0 - \frac{RT}{2F} ln\left(\frac{1}{{p_{o2}}^{0.5} p_{H2}}\right) \tag{17}$$

by substituting (10) and (17) to (20), in (16) and using the measured stack voltage, current and temperature, the only parameters that remain unknown are the partial pressure of oxygen, hydrogen and ECSA. Having the measured air mass flow rate, air pressure, and hydrogen pressure, and using equations (18) to (20), the partial pressure of oxygen and hydrogen can be calculated [43].

TABLE II
OPTIMAL SETPOINTS BASED ON THE STACK CURRENT

Current	$r_1 = \dot{m}_{cathode}$	$r_2 = p_{cathode}$	$r_3 = h_r$	$r_4 = p_{anode}$	$r_5 = T_{in}$	$r_6 = \Delta T_{thermal}$
60	25.68	1.18	0.12	0.2	68	2
100	28.15	1.28	0.12	0.2	68	2
150	34.49	1.39	0.12	0.2	68	4
200	48.098	1.61	0.12	0.2	68	8
250	56.047	1.63	0.12	0.2	68	10
300	66.82	1.75	0.12	0.2	68	12
350	75.91	1.95	0.095	0.2	68	12
400	86.45	1.97	0.095	0.2	68	12
450	94.83	2.08	0.07	0.2	68	12

$$U_{f_{O2}} = \frac{60000RTi}{4Fp_{air}\dot{m}_{air}y\%} \tag{18}$$

$$p_{O2} = (1 - U_{f_{O2}})\, y\% p_{air} \tag{19}$$

$$p_{H2} = (1 - U_{f_{H2}})\, x\% p_{fuel} \tag{20}$$

where x and y are the percentage of hydrogen and oxygen in the fuel and air respectively. The ECSA is still unknown but it can be determined using (21) as follows.

$$log\,(ECSA) = \frac{\alpha 2F}{RT}\left[V_{measurment} - E_r + \frac{RT}{\alpha 2F} log\,(i) - log\left(\left(\frac{i_{0,ref}}{A_{geo}}\right)\left(\frac{p_{O2}}{p_{O2,ref}}\right)^{1.5} exp\left(\frac{-\Delta G}{RT}\left(1 - \frac{T}{T_{ref}}\right)\right)\right) + R_{ohm} i\right] \tag{21}$$

Therefore, the temperature and ECSA are chosen as the parameters that determine the maximum power of stack. Using the experimentally validated model, multiple simulations are conducted, considering all potential combinations of the stack's temperature and ECSA. The maximum pressure is set to 2.2 bar, based on the compressor's datasheet. In addition, analysis of the real data provided by the fuel cell stack manufacturer, Powercell, has shown that the minimum allowed oxygen stoichiometry is 1.7, and the minimum allowed voltage is 220 V. Consequently, these values are taken into account during the simulation to obtain the maximum power map. For each combination of the stack temperature and ECSA, the simulation is performed by gradually increasing the current while maintaining a constant stoichiometry of 1.7 and a pressure of 2.2 bar. The simulation continues until the voltage reaches 220 V, and the maximum power achieved during this process is recorded. It is assumed that the hydrogen fuel is supplied with stoichiometry of 1.05. Furthermore, the Ohmic resistance of the stack, R_{ohm}, is adjusted to a constant value based on the experimental data of the stack. The simulation result is an offline map, which is shown in Fig. 6. The second degree polynomial function that fits the map is obtained using MATLAB and, is as follows:

$$P\,(T, ECSA) = 59410 + 36520\ T + 2906\ ECSA + 2690\ T^2 + 654.6\ T \times ECSA - 424.3\ ECSA^2 \tag{22}$$

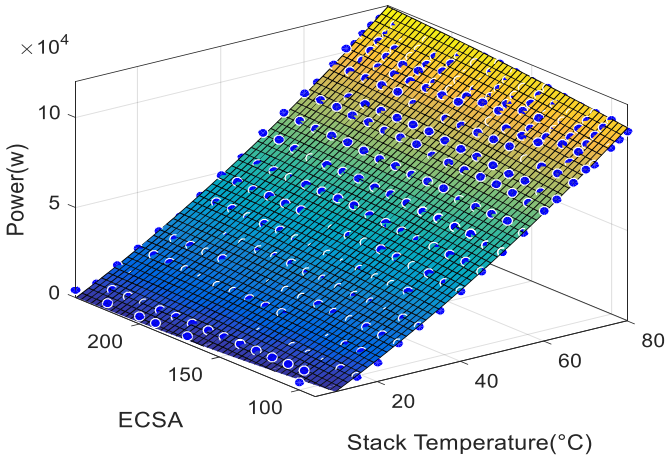

Fig. 6. Maximum gross power versus ECSA and the stack temperature

In this power map, the ECSA is estimated as an input using equation (21), while the stack temperatures are directly measured during operation. The maximum delivered gross power is the output.

2) Maximum DC/DC current setpoint: The fuel cell system supervisory controller estimates the safe current that can be drawn from the stack. In automotive applications, fuel cells are exposed to challenging scenarios of rapid load changes [44]. As a result of the dynamics of the compressor, there is a possibility of air starvation, leading to stack degradation. To protect the stack from a load current shock that causes air starvation and accelerate fuel cell degradation, the maximum safe current that can be drawn from the stack is calculated. This is accomplished by continuously monitoring the inlet air to the stack during each sampling interval. Therefore, the fuel cell supervisory controller ensures that the drawn load current is the safe current that the stack can provide. To calculate the safe current that can be drawn from the stack, equation (23) can be utilized. This equation relates the oxygen stoichiometry, λ_{O_2}, to the inlet mass flow rate to the stack and the reacted mass flow rate inside the stack.

$$\lambda_{O_2} = \frac{\dot{m}_{inlet}}{\dot{m}_{reacted}} \tag{23}$$

where $\dot{m}_{inlet}$ and $\dot{m}_{reacted}$ are the inlet and reacted mass flow rate of oxygen, respectively. The reacted oxygen mass flow rate depends on the PEMFC current and is calculated as follows:

$$\dot{m}_{O_{2reacted}}(t) = M_{O_2}\frac{n_c}{4F} I(t) \tag{24}$$

where M_{O_2} is the molar mass of oxygen, N_c, is the number of cells, I is the load current drawn from the stack, and F is the Faraday constant. By substituting (24) in (23), one has

$$I(t) = \frac{\dot{m}_{O_{2in}} 4F}{M_{O_2} n_c} \frac{1}{\lambda_{O_2}} \tag{25}$$

The stack DC/DC converter's current setpoint is calculated from (25) and knowing the inlet oxygen's mass flow rate. As the measured value represents the mass flow rate of total air, a conversion is necessary to obtain the mass flow rate of oxygen required in equation (25). By volume, dry air contains 78.09% nitrogen, 20.95% oxygen, 0.93% argon, 0.04% carbon dioxide, and small amounts of other gases. So, based on (25) to (31), the maximum safe current that can be drawn from the stack at each instant of time is calculated as indicated in (31).

$$m_{O_2} = M_{O_2} n_{O_2} \tag{26}$$

$$m_{dryair} = M_{dryair} n_{dryair} \tag{27}$$

$$\frac{m_{O_2}}{m_{dryair}} = \frac{M_{O_2} n_{O_2}}{M_{dryair} n_{dryair}} = \frac{M_{O_2}}{M_{dryair}} 0.2095 \tag{28}$$

$$\dot{m}_{total} = \dot{m}_{dryair} + \dot{m}_{vapor} = \dot{m}_{dryair} \tag{29}$$

$$\dot{m}_{dryair} = (1 + HR)\dot{m}_{dryair} \tag{30}$$

$$I(t) = \frac{\dot{m}_{total} 4F}{M_{dryair} n_c} \times \frac{0.2095}{(1 + HR)\lambda_{O_2}} \tag{31}$$

where $\dot{m}_{total}$ is the measured inlet mass flow rate, and HR is the ambient humidity ratio before the humidifier. The stoichiometry in (31), λ_{O_2}, is set to the minimum permissible stoichiometry. The current obtained in (31) will be the current setpoint and it will be imposed as the stack current by the DC/DC converter.

3) Maximum power ramp-up rate: The fuel cell stack net power ramp-up rate capability is one of the important information required by the energy management system. In this section, a procedure is presented to compute the maximum power ramp-up rate of the PEMFC. Using the relation between the current and the mass flow rate at steady state, at a constant stoichiometry, (25), one has:

$$\frac{dI(t)}{dt} = \frac{d\dot{m}_{O_{2in}}}{dt} \frac{4F}{M_{O_2} n_c} \frac{1}{\lambda_{O_2}} \tag{32}$$

Based on the information available in the compressor's datasheet, the dynamic characteristic of the compressor is as follows:

$$max(\frac{d\dot{m}_{in}}{dt}) \approx 66 \left(g/s^2\right) \tag{33}$$

So, (32) can be rewritten as follow:

$$max(\frac{dI\,(t)}{dt}) \approx \; 66 \frac{4F}{M_{O_2} n_c} \frac{1}{\lambda_{O_2}} \tag{34}$$

By substituting the constant parameters in (34), and considering the worst-case minimum stoichiometry 1.7, Eq. (34) can be rewritten as:

$$max(\frac{dI(t)}{dt}) \approx \; 66 \times 24.8594 = 1640.72(A/s) \tag{35}$$

To determine the maximum ramp-up rate of power at any given moment, it is essential to consider the following calculation:

$$\frac{\Delta P}{\Delta t} = \frac{P_2 - P_1}{\Delta t} \tag{36}$$

where P_2 is the maximum power regarding the stack's conditions of temperature and humidity. P_2 is obtained using the offline map in Fig. 6 as the maximum power, and P_1 is the measured power at each sampling time. Using Eq. (22), along with the measurement stack's current and voltage,one has

$$P_2 = P\,(T, ECSA) \tag{37}$$

$$P_1 = V_1 I_1 = V_{stack} I_{stack} \tag{38}$$

Based on (32), one has

$$\Delta t \approx \; \frac{I_2 - I_1}{\frac{dI(t)}{dt}} \tag{39}$$

To determine Δt, it is necessary to calculate the current at the maximum power point based on the stack conditions. In other words, the value of I_2 needs to be determined. Considering (32) and knowing that the maximum power will be given at the minimum specified voltage of $V_2 = 220$, the current at maximum power point can be calculated as follows:

$$I_2 = \frac{P_2}{V_2} = \frac{P\,(T, ECSA)}{220} \tag{40}$$

So, using (32) and (40), Δt is calculated and finally, the power ramp-up rate in (36) is determined.

4) Maximum instant power: Maximum instant power is the maximum net power that the system can deliver in the next sampling time $(0.01s)$. Maximum instant power is calculated based on the estimation of the maximum safe current that can be drawn from the stack in the next sampling time and considering the stack voltage in the that time. The maximum safe current is equivalent to the DC/DC setpoint current that was calculated in (31). The stack's voltage in the next sampling time is obtained by subtracting the voltage drop increment caused by activation loss, impedance losses, and concentration losses from the measured stack voltage at the current time. So, the maximum instant net power is calculated as follows:

$$P_{instantMax} = V_{nxtInst} \cdot (I_{dc-dc}) - P_{loss} \tag{41}$$

$$\begin{aligned} V_{nxtInst} = V_{measurment} - \Delta V_{Activation} - \\ \Delta V_{Impedance} - \Delta V_{Concentration} \end{aligned} \tag{42}$$

where $P_{instantMax}$ is the estimation of maximum net power that the stack can deliver in the next sampling time $(k+1)T_s$; $V_{nxtInst}$ is the estimation of stack voltage in the next sampling time $(k+1)T_s$; The impedance loss $\Delta V_{Impedance}$ is calculated as follows:

$$\Delta V_{Impedance} = R_{ohm}(I_{dc-dc} - I_{stack}) \tag{43}$$

where R_{ohm} is the Ohmic resistance of the stack obtained based on the simulation of the validated model; $\Delta V_{Activation}$ and $\Delta V_{Concentration}$ are neglected. Where R_{ohm} represents the Ohmic resistance of the stack, which is obtained through simulation using the validated model. Assuming operation in the linear region of the polarization curve, the voltage change between sampling times is attributed solely to the Ohmic voltage drop, while disregarding other voltage drop factors such as activation, $\Delta V_{Activation}$, and concentration losses $\Delta V_{Concentration}$.

IV. Run Mode Control Loop and Simulation Results

In Section III, the blocks of the fuel cell system supervisory controller were explained, elucidating their role in the operation of the integrated system, as well as providing a detailed clarification of their inputs and outputs. In this section, the purpose is to evaluate the performance of the proposed supervisory controller integrated with the stack model and subsystems models for a standard load profile.

A. Run state control loop

As explained in the section of state machine architecture, there are ten discrete states for the fuel cell system. In the following scenario, it is assumed that the state machine is in the "Run" state, and the startup procedures have been executed correctly. During Run state, the setpoint generator updates the subsystems' references based on the requested gross power from the vehicle side. The vehicle propulsion requested net power is added with the estimation of compressor power consumption, and it is converted to the equivalent current using the polarization curve of the stack. Subsequently, this current is fed to the optimal setpoint generator map. The power limit calculator unit also generates the DC/DC converter current reference based on the measurement mass flow of air. Furthermore, it provides information to the energy management system regarding the available net power that the stack can deliver, as extensively explained in Section III-C. During the Run state, the state machine receives the subsystems' setpoints from the optimal setpoint generator, along with the DC/DC setpoint current from the power limit calculator. It then distributes these setpoints to the various subsystems and the DC/DC converter. The block diagram in Fig. 7 shows the integration of the fuel cell system supervisory controller with other auxiliary subsystems such as the anode subsystem, cathode subsystem, thermal subsystem, FC stack, vehicle control unit, propulsion parts, and diagnosis subsystem. In the Run state, the following

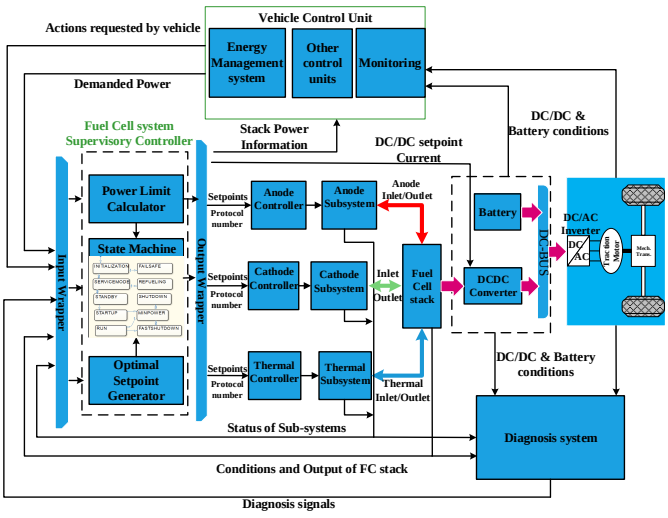

Fig. 7. Block diagram of the proposed fuel cell system supervisory controller integrated with fuel cell system

procedure is executed in each iteration of the system operation, i.e., every 0.01 s.

- The driver decides to accelerate or decelerate.
- Considering the requested net power by the traction motor, the state of charge of the battery, and the implemented energy management algorithm, the vehicle control unit sends the net power request to the fuel cell system.
- Using the compressor power consumption map, the compressor consumption is estimated and is added to the requested net power to have the gross power.

$$P_{gross} = P_{net} + P_{compressor} \tag{44}$$

- The requested gross power is converted to current using the static polarization curve of the stack, and the Optimal Setpoint Generator unit generates the optimal setpoints for the three subsystems corresponding to the load current.
- The generated optimal setpoints of the three subsystems are sent to the subsystems' local controllers through the state machine.
- The Power Limit Calculator unit calculates the available net power and power ramp-up capability by considering the stack temperature, stack hydration condition, voltage, current, and estimates of other power losses in the system, such as compressor and fans power consumption. The Power Limit Clculator unit directly sends this information as the stack net power information to the vehicle control unit. Furthermore, the DC/DC converter setpoint current is calculated inside this unit, and the state machine sends this information to the DC/DC converter as the DC/DC current setpoint.

B. Simulation results and analysis

The simulation is conducted using the standard driving cycles. Driving cycles address the change of speed in a specific period and its principal characteristics such as duration, average speed, maximum speed, and the dynamics velocity changes of the vehicle. The driving cycle ought to be designed to represent a realistic traffic conditions [45]. In this simulation, a driving cycle corresponding to highway driving is selected. The simulation parameters for the car are as follows: m_{car} (mass of car) = 2700, A_{car} (frontal surface area) = 2 m^2, ρ (air density) = 1.2 kg/m^3, c_R (rolling resistance) = 0.015, c_D (drag coefficient) = 0.03.

1) Vehicle test driving cycle: The Common Artemis Driving Cycles (CADC) are chassis dynamometer procedures that were developed as part of the European Artemis project. These driving cycles were created based on statistical analysis of a large database of real-world driving patterns in Europe. Fig. 8 shows the speed profile of one of the driving cycles from this family. The forces acting on the vehicle include internal resistance, tire resistance, and air resistance. The total drag force is estimated by (45).

$$F_D = \frac{1}{2}\rho c_D A_{car} V^2 + c_R m_{car} g \tag{45}$$

where c_R and c_D are rolling resistance and drag coefficients, respectively. The variables m_{car}, A_{car}, and ρ represent the mass of the vehicle, the frontal surface area of the vehicle,

and the density of air, respectively. The power required to accelerate to a given speed is estimated as (46)

$$P_{required} = F_D V_{car} + m_{car} a_{car} V_{car} \tag{46}$$

where a_{car}, V_{car} are the acceleration and speed of the vehicle. The required net power and gross power corresponding to the Artemis130 profile is shown in Fig. 8. The estimation of the compressor power consumption is added to the net demanded power to obtain the gross demanded power. The zoomed-in part between t = 279 s to t = 289 s is shown in Fig. 8. It highlights the difference between the requested net power and the gross power. In this study, it is assumed that there is no hybridization, meaning that all the power is solely provided by the fuel cell. This assumption is made to test the system under the worst-case scenario.

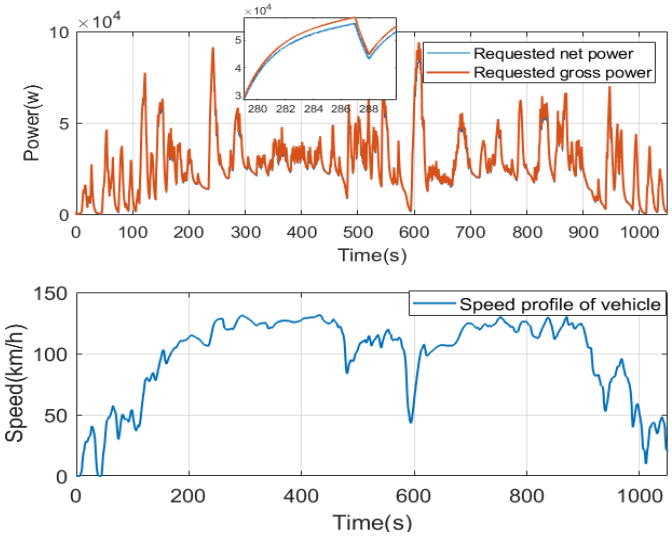

Fig. 8. Artemis130 profile corresponding net and gross power demand and speed profile

2) Stack current: In section III-C2, it was explained that in order to protect the stack from sudden load current shocks that can lead to air starvation and increased fuel cell degradation, the stack current is determined as the minimum value between the computed current based on the mass flow measurement using equation (31) and the current obtained from the polarization curve. This approach takes into consideration the dynamic behavior of the compressor and ensures that the stack operates within safe limits.

$$I_{st}(t) = min(I_{Massflow\ estimation}, I_{polarization\ Curve}) \tag{47}$$

Fig. 9 illustrates the alignment between the DC/DC setpoint current, the stack current, and the computed current based on the polarization curve. It is assumed that the DC/DC converter controller works perfectly and is able to tracks the given current setpoint. In Fig. 9, it is clear that the dynamic of the compressor affects the current that is sent to the DC/DC converter as the setpoint. The DC/DC setpoint current, the red line, follows the load current computed by the maps, blue line, with a time delay. Therefore, the air starvation is avoided and always a safe current is applied to the stack, corresponding to the mass flow of air at the inlet of stack.

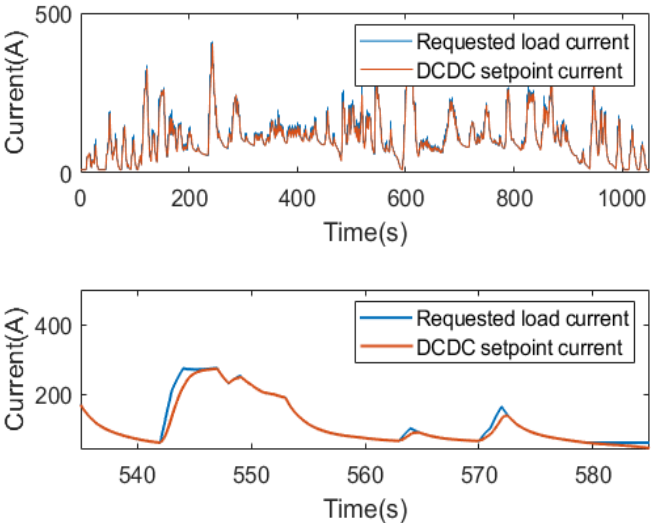

Fig. 9. DC/DC converter setpoint or the stack current and optimal setpoint generator current in upper and the zoomed part between t = 535 s and t = 585 s in the lower graph

3) The Subsystems local controllers performance : In this section, the simulation results of the subsystems setpoints and their local controller's ability in achieving the desired setpoint will be discussed. To meet the requirements of the project, three setpoints are defined for the cathode subsystem. Regarding the requested net power by the vehicle control unit, the optimal setpoint generator produces the three setpoints (inlet mass flow rate of air, inlet air pressure, and humidity ratio), which are then sent to the cathode local controller. The setpoints are shown in Fig. 10. The simulation results indicate that the cathode subsystem has satisfactory behavior, and the three variables of inlet air pressure, mass flow rate, and humidity ratio of inlet air closely track their respective setpoints. The anode subsystem provides the flow of hydrogen

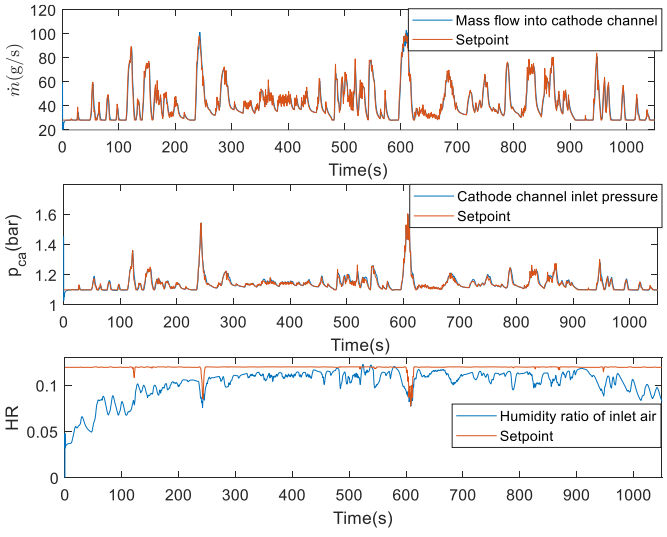

Fig. 10. Three setpoints of the cathode subsystem and the actual values. Inlet air mass flow rate, Inlet air pressure, Inlet air humidity ratio

from the H_2 tank to the fuel cell. The anode subsystem

controller controls the anode channel inlet pressure to satisfy the manufacture's requirements. The anode subsystem uses an injector-ejector to recirculate the unconsumed hydrogen. The generated setpoint and the performance of the anode subsystem controller are depicted in Fig. 11. As Fig. 11 indicates, the anode channel inlet pressure precisely follows the setpoint, demonstrating the proper functioning of the local controller in the anode subsystem. The H_2 flow from the tank

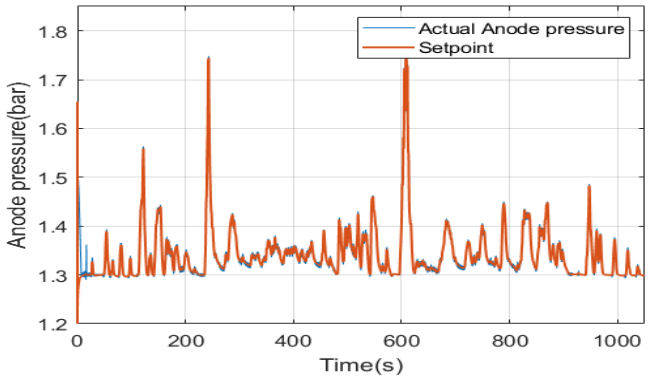

Fig. 11. Anode channel pressure setpoint and the actual anode pressure

is shown in Fig. 12. The PEMFC in this project is designed

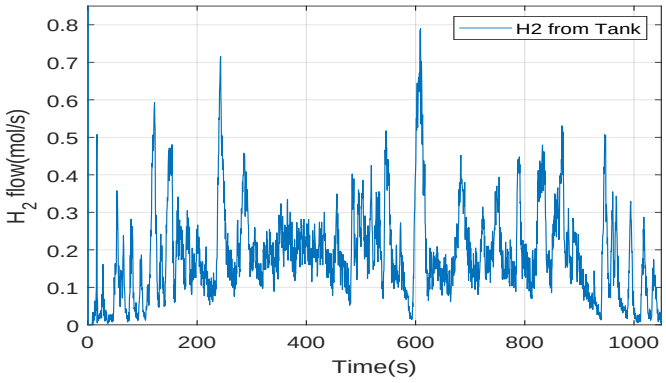

Fig. 12. H_2 flux from the pressurized Tank

to operate with a maximum temperature difference between the inlet and outlet under normal operating conditions from 68° to 80° Celsius. The thermal subsystem is responsible for controlling the stack temperature. The thermal subsystem uses water as the liquid coolant, and during normal stack operation, the coolant's inlet temperature must be maintained at $68°C$. The outlet coolant has to be $2°C$ to $12°C$ higher than the inlet temperature. So, the outlet coolant temperature has to be in the range of $70°C$ to $80°C$. The thermal subsystem has two setpoints as follows:

- Inlet coolant temperature
- Outlet coolant temperature

The setpoints of the thermal subsystem and its local controller performance are shown in Fig. 13. According to the simulation results, the coolant's inlet temperature closely tracks the setpoint of $68°C$. The temperature difference between inlet and outlet coolant, ΔT, is the second setpoint that the thermal subsystem has to follow. Due to the slow dynamics of the temperature, it takes a longer time to reach the setpoint.

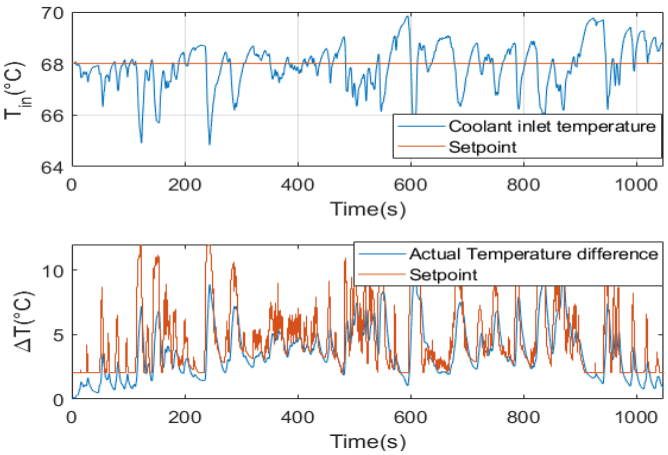

Fig. 13. Thermal subsystem setpoints and setpoint achievement of thermal subsystem

4) Stack output power and efficiency: The output gross power of the stack is shown in Fig. 14a. The simulation results show the stack has the capability to produce the power demanded by the vehicle. The compressor in the cathode subsystem is considered the main parasitic loss in the system. The power consumption by all the pumps, fan, and other types of equipment in the three subsystems are negligible. So, the lost power is subtracted from the stack's gross produced power to obtain the net power as follows.

$$P_{net}=P_{gross}-P_{loss}=V_{stack}I_{stack}-P_{Compressor} \quad (48)$$

As Fig. 14a showed, the stack output power is equal to the vehicle's demanded net power plus the compressor power. In accordance with the manufacturer's requirements, the inlet airflow to the stack has a minimum value. Even when the vehicle's requested net power is zero, there exists a minimum value for the stack current and, correspondingly, a minimum value of the reactants flows. So, the stack output power, red line in Fig. 14a (a) , has a higher value than the requested gross power by the vehicle, blue line in Fig. 14a (a) when the net power demanded by the vehicle is zero. The compressor power consumption is shown in Fig. IV-B4.

5) Power limit calculator outputs: Providing information about the available range of net power that the fuel cell stack can deliver is crucial for the energy management system. This information enables the system to effectively allocate the requested net power between the battery and the fuel cell. The power limit calculator (PLC) unit provides this information about the stack, explained in section III-C. Fig. 15 shows the maximum net power, maximum instant net power, and maximum power ramp-up rate.

The overall instant fuel cell system efficiency considering the high heating value of hydrogen, $141.7MJ/Kg$, is computed using (14) and is shown in Fig. 16. The overall system efficiency considering subsystem losses is around 55% which is satisfactory. In order to compare the optimal scenario with a non-optimal scenario, constant setpoints such as air stoichiometry $\lambda_{O2} = 3$, cathode inlet air pressure, $p_{ca} = 1.3$ bar, coolant

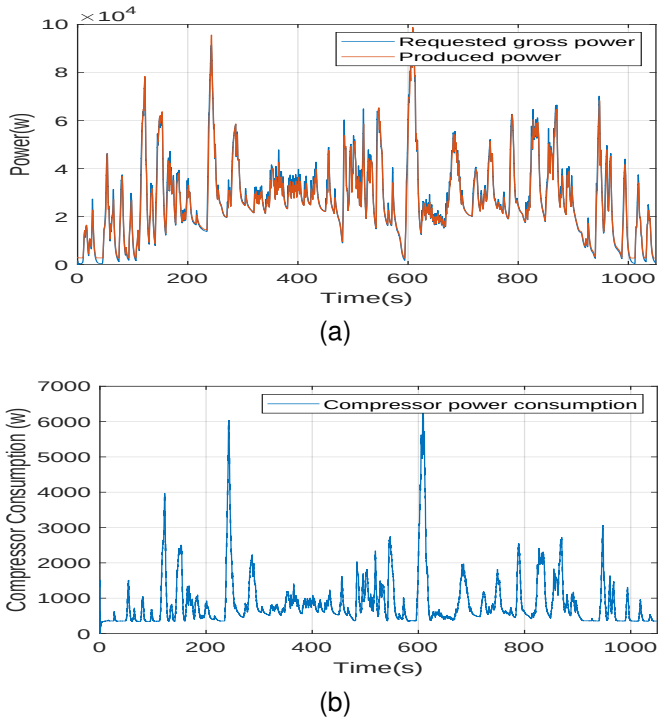

Fig. 14. (a)Output power of the stack.(b) Compressor power consumption

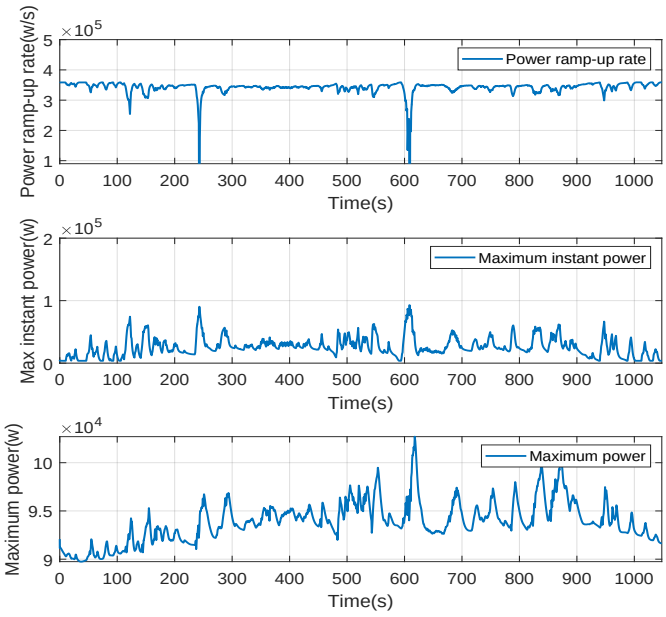

Fig. 15. Stack power information: Maximum net power, Maximum instant net power, Power ramp-up rate

inlet temperature, $T = 68°C$, temperature difference between inlet and outlet coolant, $\Delta T = 5°C$, and humidity ratio of inlet air *HR* = 0.12 are considered. These non-optimal values of ΔT and p_{ca} are selected as the average of the permissible range. The λ_{O2} is selected in a way that covers all ranges of current while preventing air starvation. . The utilization of the optimal setpoint generator in the fuel cell system indicates a reduction of around 4% in the input available power from the H_2 tank compared to the utilization of non-optimal setpoints. This outcome highlights the effectiveness of the proposed optimal

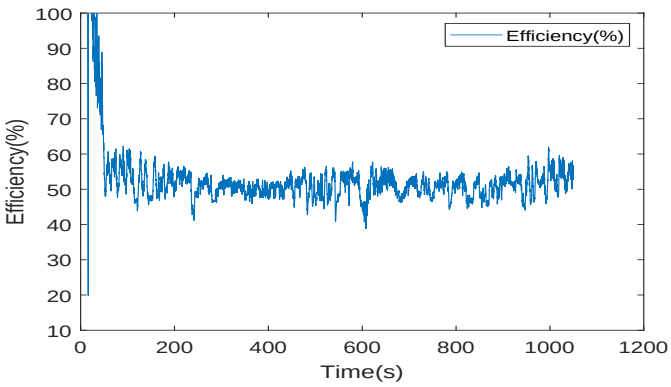

Fig. 16. Fuel cell system overall efficiency

setpoint generator within the proposed supervisory controller.

V. Conclusion

In this study, a PEMFC system supervisory controller for an automotive application has been designed, implemented, and validated through simulation. The proposed fuel cell supervisory controller integrates three main parts: a state machine, an optimal setpoint generator, and a power limit calculator. Simulation results were obtained using an integrated model of the experimentally validated stack model with INN-BALANCE developed prototype and the subsystems models with their local controllers. The system performance was studied with the Common Artemis Driving Cycle 130 profile in the Run state of the state machine. The simulation results show how these three software elements can work together in order to determine optimal operating conditions and compute the available fuel cell range of power in Run state. In addition, the subsystems local controllers achieved their setpoints properly. Furthermore, the results indicate that the power demanded by the vehicle is satisfactorily fulfilled for the selected driving cycle with good efficiency, showing an improvement of approximately 4% compared to the non-optimal strategy. The key points of this study can be highlighted as follows:

- An equivalent electric circuit model of the distributed parameters membrane model was proposed. This model is used in the galvanostatic mode of operation in which the load current acts as an input disturbance to the stack. As the automotive PEMFC system works in galvanostatic mode during the Run state, this electric circuit model allows to emulate the behavior of the distributed parameters model in the galvanostatic mode, and it is compatible with an automotive application.
- A complex experimentally validated model of all the subsystems including valves, fans, and equipment that exist in a real fuel cell based vehicle has been utilized in the design and simulation of the supervisory controller. This model takes into account the important aspects and behaviors of the system operation that are generally neglected in the traditional simple models and, the proposed supervisory controller has shown satisfactory results with this model. The sampling time for the simulation is set

to 0.01 s, which is the standard sampling time for the automotive application.

- The simulation results have shown that the three parts of the proposed supervisory controller are properly coordinated. Specifically, apart from determining the optimal operating conditions and setpoints for the balance of plant subsystems in the Run state, it provides a framework that allows to handle the fuel cell system processes and execute the Start-up and Shutdown procedures.
- The stack power information that the vehicle's energy management system (EMS) needs to divide the requested power between the battery and the fuel cell system were determined by the supervisory controller. Using this information, the requested power from the fuel cell system does not exceed the capability of the system, which is very important to minimize stack degradation and/or damage.

REFERENCES

[1] K.-Y. Shen, S. Park, and Y.-B. Kim, "Hydrogen utilization enhancement of proton exchange membrane fuel cell with anode recirculation system through a purge strategy," *International Journal of Hydrogen Energy*, vol. 45, no. 33, pp. 16 773–16 786, 2020.

[2] E. Commission and D.-G. for Climate Action, *Going climate-neutral by 2050 : a strategic long-term vision for a prosperous, modern, competitive and climate-neutral EU economy*. Publications Office, 2019.

[3] S. Changizian, P. Ahmadi, M. Raeesi, and N. Javani, "Performance optimization of hybrid hydrogen fuel cell-electric vehicles in real driving cycles," *International Journal of Hydrogen Energy*, vol. 45, no. 60, pp. 35 180–35 197, 2020.

[4] X. Guo, H. Zhang, J. Yuan, J. Wang, J. Zhao, F. Wang, H. Miao, and S. Hou, "Energetic and exergetic analyses of a combined system consisting of a high-temperature polymer electrolyte membrane fuel cell and a thermoelectric generator with thomson effect," *International Journal of Hydrogen Energy*, vol. 44, no. 31, pp. 16 918–16 932, 2019.

[5] F. S. Nanadegani, E. N. Lay, A. Iranzo, J. A. Salva, and B. Sunden, "On neural network modeling to maximize the power output of pemfcs," *Electrochimica Acta*, vol. 348, p. 136345, 2020.

[6] J. Wang, H. Wang, and Y. Fan, "Techno-economic challenges of fuel cell commercialization," *Engineering*, vol. 4, no. 3, pp. 352–360, 2018.

[7] G. Wang, F. Huang, Y. Yu, S. Wen, and Z. Tu, "Degradation behavior of a proton exchange membrane fuel cell stack under dynamic cycles between idling and rated condition," *international journal of hydrogen energy*, vol. 43, no. 9, pp. 4471–4481, 2018.

[8] H. Chen, X. Zhao, T. Zhang, and P. Pei, "The reactant starvation of the proton exchange membrane fuel cells for vehicular applications: A review," *Energy conversion and management*, vol. 182, pp. 282–298, 2019.

[9] R. O'hayre, S.-W. Cha, W. Colella, and F. B. Prinz, *Fuel cell fundamentals*. John Wiley & Sons, 2016.

[10] X.-G. Yang, Q. Ye, and P. Cheng, "Matching of water and temperature fields in proton exchange membrane fuel cells with non-uniform distributions," *international journal of hydrogen energy*, vol. 36, no. 19, pp. 12 524–12 537, 2011.

[11] S. Strahl, A. Husar, P. Puleston, and J. Riera, "Performance improvement by temperature control of an open-cathode pem fuel cell system," *Fuel Cells*, vol. 14, no. 3, pp. 466–478, 2014.

[12] Y.-X. Wang, F.-F. Qin, K. Ou, and Y.-B. Kim, "Temperature control for a polymer electrolyte membrane fuel cell by using fuzzy rule," *IEEE Transactions on Energy Conversion*, vol. 31, no. 2, pp. 667–675, 2016.

[13] L. Huang, J. Chen, Z. Liu, and M. Becherif, "Adaptive thermal control for pemfc systems with guaranteed performance," *International Journal of Hydrogen Energy*, vol. 43, no. 25, pp. 11 550–11 558, 2018.

[14] L. Sun, Y. Jin, and F. You, "Active disturbance rejection temperature control of open-cathode proton exchange membrane fuel cell," *Applied energy*, vol. 261, p. 114381, 2020.

[15] C. Lebreton, M. Benne, C. Damour, N. Yousfi-Steiner, B. Grondin-Perez, D. Hissel, and J.-P. Chabriat, "Fault tolerant control strategy applied to pemfc water management," *International Journal of Hydrogen Energy*, vol. 40, no. 33, pp. 10 636–10 646, 2015.

[16] C. Damour, M. Benne, B. Grondin-Perez, J.-P. Chabriat, and B. G. Pollet, "A novel non-linear model-based control strategy to improve pemfc water management–the flatness-based approach," *international journal of hydrogen energy*, vol. 40, no. 5, pp. 2371–2376, 2015.

[17] H. Fu, J. Shen, L. Sun, and K. Y. Lee, "Fuel cell humidity modeling and control using cathode internal water content," *International Journal of Hydrogen Energy*, vol. 46, no. 15, pp. 9905–9917, 2021.

[18] T.-H. Kim, S.-H. Kim, W. Kim, J.-H. Lee, and W. Choi, "Development of the novel control algorithm for the small proton exchange membrane fuel cell stack without external humidification," in *2010 Twenty-Fifth Annual IEEE Applied Power Electronics Conference and Exposition (APEC)*. IEEE, 2010, pp. 2166–2173.

[19] J. T. Pukrushpan, A. G. Stefanopoulou, and H. Peng, "Modeling and control for pem fuel cell stack system," in *Proceedings of the 2002 American Control Conference (IEEE Cat. No. CH37301)*, vol. 4. IEEE, 2002, pp. 3117–3122.

[20] A. Dalvi and M. Guay, "Control and real-time optimization of an automotive hybrid fuel cell power system," *Control Engineering Practice*, vol. 17, no. 8, pp. 924–938, 2009.

[21] Q. Li, W. Yang, L. Yin, and W. Chen, "Real-time implementation of maximum net power strategy based on sliding mode variable structure control for proton-exchange membrane fuel cell system," *IEEE Transactions on Transportation Electrification*, vol. 6, no. 1, pp. 288–297, 2020.

[22] M. Fayyazi, P. Sardar, S. I. Thomas, R. Daghigh, A. Jamali, T. Esch, H. Kemper, R. Langari, and H. Khayyam, "Artificial intelligence/machine learning in energy management systems, control, and optimization of hydrogen fuel cell vehicles," *Sustainability*, vol. 15, no. 6, p. 5249, 2023.

[23] H. Zhang, Y. Wang, D. Wang, and Y. Wang, "Adaptive robust control of oxygen excess ratio for pemfc system based on type-2 fuzzy logic system," *Information Sciences*, vol. 511, pp. 1–17, 2020.

[24] M. Gheisarnejad, J. Boudjadar, and M.-H. Khooban, "A new adaptive type-ii fuzzy-based deep reinforcement learning control: Fuel cell air-feed sensors control," *IEEE Sensors Journal*, vol. 19, no. 20, pp. 9081–9089, 2019.

[25] M. Sarmiento-Carnevali, M. Serra, and C. Batlle, "Distributed parameter model-based control of water activity and concentration of reactants in a polymer electrolyte membrane fuel cell," *International Journal of Hydrogen Energy*, vol. 42, no. 42, pp. 26 389–26 407, 2017.

[26] J. Luna, E. Usai, A. Husar, and M. Serra, "Enhancing the efficiency and lifetime of a proton exchange membrane fuel cell using nonlinear model-predictive control with nonlinear observation," *IEEE transactions on Industrial Electronics*, vol. 64, no. 8, pp. 6649–6659, 2017.

[27] J. Wishart, Z. Dong, and M. Secanell, "Optimization of a pem fuel cell system based on empirical data and a generalized electrochemical semi-empirical model," *Journal of Power Sources*, vol. 161, no. 2, pp. 1041–1055, 2006.

[28] J. Wu, Q. Liu, and H. Fang, "Toward the optimization of operating conditions for hydrogen polymer electrolyte fuel cells," *Journal of Power Sources*, vol. 156, no. 2, pp. 388–399, 2006.

[29] J. A. Luna Pacho, "Development of control systems and state observers for efficiency and durability improvement in pem fuel cell based systems," 2017.

[30] I.-S. Sorlei, N. Bizon, P. Thounthong, M. Varlam, E. Carcadea, M. Culcer, M. Iliescu, and M. Raceanu, "Fuel cell electric vehicles—a brief review of current topologies and energy management strategies," *Energies*, vol. 14, no. 1, p. 252, 2021.

[31] A. M. Fernandez, M. Kandidayeni, L. Boulon, and H. Chaoui, "An adaptive state machine based energy management strategy for a multi-stack fuel cell hybrid electric vehicle," *IEEE Transactions on Vehicular Technology*, vol. 69, no. 1, pp. 220–234, 2019.

[32] (2019) Inn-balance project description. [Online]. Available: https://www.innbalance-fch-project.eu/

[33] P. Ahmadi, S. H. Torabi, H. Afsaneh, Y. Sadegheih, H. Ganjehsarabi, and M. Ashjaee, "The effects of driving patterns and pem fuel cell degradation on the lifecycle assessment of hydrogen fuel cell vehicles," *International Journal of Hydrogen Energy*, vol. 45, no. 5, pp. 3595–3608, 2020.

[34] M. Nöst, C. Doppler, M. Klell, and A. Trattner, "Thermal management of pem fuel cells in electric vehicles," in *Comprehensive Energy Management-Safe Adaptation, Predictive Control and Thermal Management*. Springer, 2018, pp. 93–112.

[35] J. Luna, S. Jemei, N. Yousfi-Steiner, A. Husar, M. Serra, and D. Hissel, "Nonlinear predictive control for durability enhancement and efficiency improvement in a fuel cell power system," *Journal of Power Sources*, vol. 328, pp. 250–261, 2016.

[36] M. Mangold, A. Bück, and R. Hanke-Rauschenbach, "Passivity based control of a distributed pem fuel cell model," *Journal of Process Control*, vol. 20, no. 3, pp. 292–313, 2010.
[37] F. Barbir, *PEM fuel cells: theory and practice*. Academic press, 2012.
[38] W. Neubrand, *Modeling and simulation of electromembrane processes*. Logos-Verlag, 1999.
[39] Z. Dong, X. Huang, Y. Dong, and Z. Zhang, "Multilayer perception based reinforcement learning supervisory control of energy systems with application to a nuclear steam supply system," *Applied Energy*, vol. 259, p. 114193, 2020.
[40] F. Dittmann, K. Geramani, V. Fäßler, and S. Damiani, "State machine based method for consolidating vehicle data," in *International Embedded Systems Symposium*. Springer, 2009, pp. 1–11.
[41] M. Zhang, N. Li, A. Girard, and I. Kolmanovsky, "A finite state machine based automated driving controller and its stochastic optimization," in *Dynamic Systems and Control Conference*, vol. 58288. American Society of Mechanical Engineers, 2017, p. V002T07A002.
[42] J. C. Gómez, M. Serra, and A. Husar, "Controller design for polymer electrolyte membrane fuel cell systems for automotive applications," *International Journal of Hydrogen Energy*, 2021.
[43] S. N. Motapon, O. Tremblay, and L.-A. Dessaint, "Development of a generic fuel cell model: application to a fuel cell vehicle simulation," *International Journal of Power Electronics*, vol. 4, no. 6, pp. 505–522, 2012.
[44] T. Zhang, P. Wang, H. Chen, and P. Pei, "A review of automotive proton exchange membrane fuel cell degradation under start-stop operating condition," *Applied energy*, vol. 223, pp. 249–262, 2018.
[45] J. L. Xue, "Analysis of driving cycles for emission test of light-duty vehicles in china," in *Advanced Materials Research*, vol. 616. Trans Tech Publ, 2013, pp. 1154–1160.

VI. Biography Section

Ali Molavi is a Ph.D. candidate of Control Engineering in the Institute de Robòtica i Informàtica Industrial at the Polytechnic University of Catalonia. His research interests are control theory, model predictive control, fuel cell hybrid vehicles.

Maria Serra Prat received the Physics Degree from the Barcelona University in 1995 and the Ph.D. degree in Chemical Engineering from the Polytechnic University of Catalonia in 2000. She is currently the Head of the Automatic Control Group in the Institut de Robotica i Informatica Industrial and an Associate Professor with the Department of Automatic Control. She is also the director of the Hydrogen Research Specific Center of UPC (CER-H2). Her research interests are modeling and control of complex systems, focusing on energy generation and hydrogen systems. systems.

Attila Peter Husar received his Bachelors and M.Sc. degrees in Mechanical Engineering from the University of Miami, Coral Gables, FL, and his Ph.D. at the Polytechnic University of Catalonia, Barcelona, Spain, where he has designed and built a multitude of fuel cell test stations, systems, and hydrogen technologies laboratories. He has spent his more than 20-year engineering career directly involved in the development of PEM fuel cells and systems. He has co-authored more than 25 publications in international scientific journals. He is currently the scientific coordinator of the UPC Hydrogen Lab.